THE JOURNAL OF PHYSICAL CHEMISTRY A

 VOLUME 105, NUMBER 50, DECEMBER 20, 2001

LETTERS

Ultrafast Diffraction of Transient Molecular Structures in Radiationless Transitions

Vladimir A. Lobastov, Ramesh Srinivasan, Boyd M. Goodson, Chong-Yu Ruan, Jonathan S. Feenstra, and Ahmed H. Zewail*

Laboratory for Molecular Sciences, Arthur Amos Noyes Laboratory of Chemical Physics, California Institute of Technology, Pasadena, California 91125

Received: October 3, 2001

Radiationless transitions in molecules are ubiquitous in photophysical, chemical, and biological systems. Because such transitions are usually ultrafast in nature, the determination of transient structures is extremely difficult, particularly for complex molecules with many degrees of freedom. Here, we report the direct determination of the *molecular structure* during the ultrafast, nonradiative transition in aromatic pyridine, excited above the so-called channel three threshold, which marks the onset of an anomalous decay. The approach we invoked is ultrafast electron diffraction (UED), developed in this laboratory to image transient molecular structures in real time. The diffraction results reveal the breakage of "old bonds" near 1.4 and 2.4 Å and the formation of "new bonds" near 1.3 and 1.5 Å and at distances greater than ∼3.5 Å, thus permitting the dominant intermediate species to be identified. Unexpectedly, a ring-opened diradical structure resulting from C−N bond scission was observed and was found to form with a rate of $(17\ \text{ps})^{-1}$. This hitherto unknown intermediate must be considered as a new channel for energy dissipation in pyridine and possibly analogous molecules. These results represent a clear demonstration of the potential of UED for studying structural dynamics of radiationless transitions in complex molecular systems.

Aromatic molecules such as benzene and pyridine are known to exhibit a dramatic decrease in their fluorescence quantum yield, with concomitant passage through a rapid nonradiative relaxation process,[1−3] when prepared with enough vibrational energy in the excited singlet (S_1) state[1]; for pyridine, this onset occurs at ∼1600 cm^{-1} above the S_1 origin.[4] Several theoretical (for example, see refs 5 and 6) and experimental (for example, see refs 4 and 7−10) investigations have addressed this phenomenon, termed the "channel three" process, since it was first observed in benzene thirty years ago.[11] High-resolution spectroscopic studies[10] of the bound molecule have shown the spectral signature in line broadening and states coupling. Whereas spectroscopy probes energy level populations and perturbations, ultrafast electron diffraction (UED) has the capability of mapping all internuclear coordinates, from the initial to the final structure, on the time scale of the change; for work done in this laboratory, see, for example, refs 12−14.

In UED, a femtosecond light pulse transfers molecules from the ground-state potential energy surface up to an excited surface, and the sequentially delayed ultrashort electron pulses then probe the ensuing structural dynamics. We excited isolated pyridine molecules with UV femtosecond (fs) pulses and probed the consequent structural evolution with our third-generation UED apparatus,[13,14] the specifics of which will be described in greater detail in a future publication.

Briefly, the output from an amplified Ti:sapphire laser system (380 μJ, 120 fs, 267 nm, 1 kHz repetition rate) was split into two beams; the more powerful beam (∼150 μJ) was directed into the scattering chamber to initiate the reaction, whereas the weaker beam (∼ 5 μJ) was directed into a delay line and then

* To whom correspondence should be addressed. E-mail: zewail@caltech.edu.

10.1021/jp013705b CCC: $20.00
Published on Web 11/09/2001

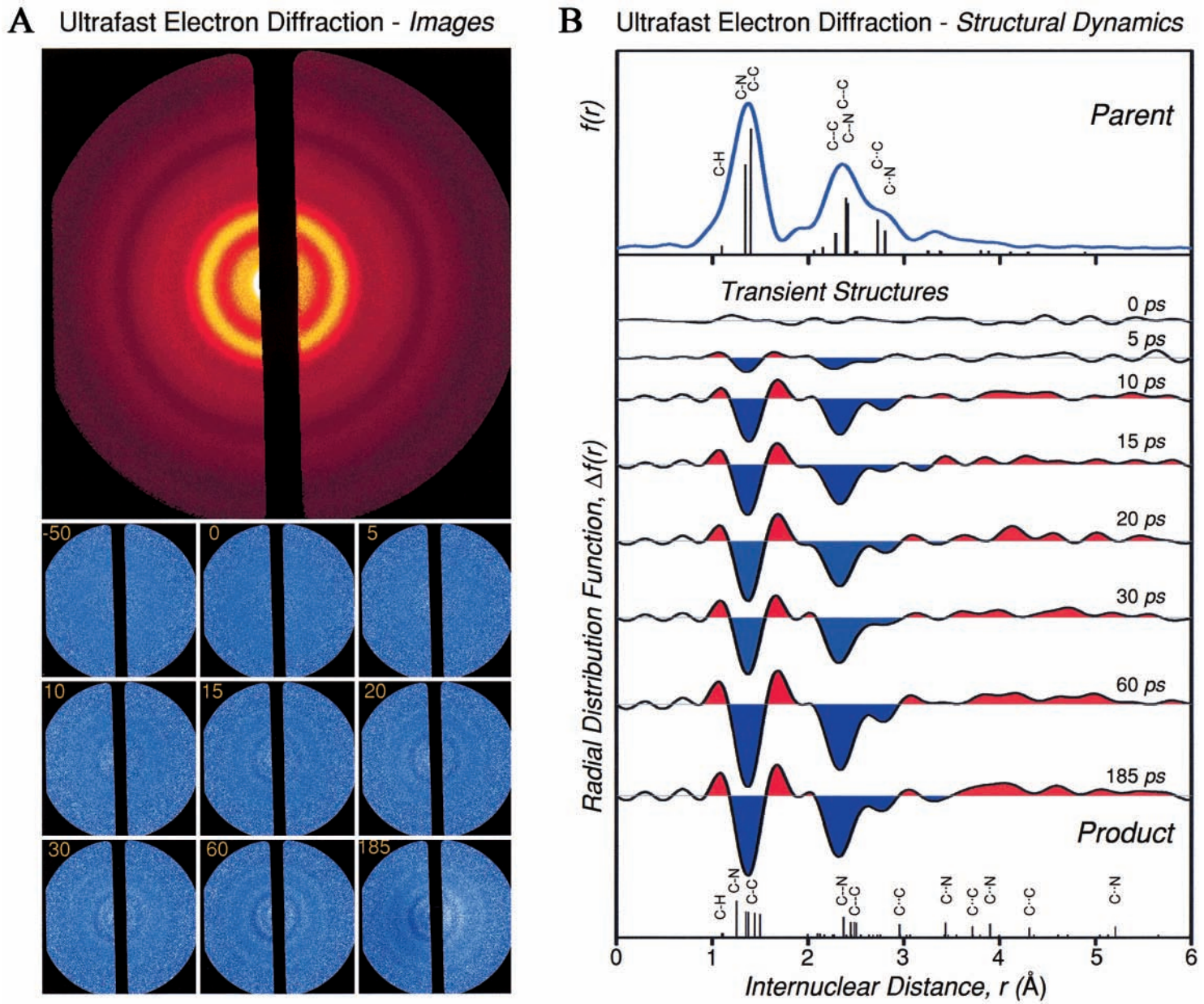

Figure 1. Ultrafast electron diffraction images and corresponding radial distribution curves. (a) Ground-state diffraction image of pyridine (top); Time-resolved diffraction-difference images (bottom). (b) Corresponding radial distribution $f(r)$ curves for parent (top) and $\Delta f(r; t)$ curves (bottom). The vertical lines indicate the relative contributions from various internuclear pairs, with the height of each line scaling with $(Z_iZ_j)/r_{ij}$ multiplied by the degeneracy (Z is the nuclear charge and r_{ij} is the internuclear distance). The blue highlighted regions represent net depletion of internuclear pairs ("old bonds"), whereas the red highlighted regions correspond to internuclear pairs with increasing population ("new bonds").

focused onto a back-illuminated silver photocathode to generate electron pulses via the photoelectric effect (30 kV; de Broglie wavelength, $\lambda = 0.067$ Å; ~25 000 electrons per pulse at ~3.5 ps). The molecular sample was introduced into the chamber via a jet expansion source; the nozzle temperature was maintained at 130 °C. The diffracted electrons were detected with a low-noise CCD camera (active s range ~1.5−18.5 Å^{-1}; see below). The reaction zero-of-time was determined by the ion-induced lensing technique[15] using CF_3I gas (Aldrich, 99%). Pyridine (EM Science, 99.98%) was degassed with three freeze−pump−thaw cycles; high-purity xenon (Spectra Gases, 99.999%) was used as an atomic reference gas.[13,16]

Two-dimensional diffraction images were radially averaged to generate 1D total intensity curves, from which experimental modified molecular scattering [$sM(s)$] curves were obtained:

$$sM(s) = s\frac{I_M(s)}{|f_a||f_b|} \quad (1)$$

where s is the momentum transfer parameter given by $s = (4\pi/\lambda)\sin(\theta/2)$ and θ is the scattering angle. $I_M(s)$ is the molecular scattering intensity consisting of contributions from all atom−atom pairs; f_a and f_b are the elastic scattering amplitudes for two chosen atoms in the molecule (usually atoms with relatively high atomic number). Theoretical $sM(s)$ curves derived from structural parameters were then compared with the experimental data. The corresponding radial distribution [$f(r)$] curves were obtained via Fourier (sine) transform of the $sM(s)$ curves:

$$f(r) = \int_0^{s_{max}} sM(s)\sin(sr)\exp(-ks^2)\,ds \quad (2)$$

where r is the interatomic distance and k is the damping constant that accounts for the finite s range of the detector.

Figure 1a shows the 2D ground-state diffraction image of pyridine (top). The peaks in the corresponding radial distribution $f(r)$ curve (Figure 1b, top) directly reflect the relative density of various internuclear separations in pyridine; for example, the covalent C−C and C−N distances occur at ~1.3 Å, the second-nearest neighbor C- -C and C- -N distances at ~2.3 Å, and the third-nearest neighbor C··C and C··N distances at ~2.8 Å. The curve is in excellent agreement with *steady-state* electron diffraction data[17] and previous quantum chemical calculations.[18]

To resolve the structural changes during the course of the reaction, we collected UED images for a range of time delays from −90 to +185 ps. The temporal diffraction-difference method,[19] whereby UED data obtained at a negative time is subtracted pixel-by-pixel from data taken at positive times, was employed to isolate the net change in the diffraction patterns obtained over the course of the reaction. The time-dependent difference signals are comprised equally of (1) negative contributions from the depleted parent structures and (2) positive contributions from the product structures, thereby permitting the relative fractions of the parent and product structures to be determined as a function of time. The 2D diffraction-difference images clearly exhibit the emergence of periodic ring patterns (Figure 1a, bottom), whose intensity becomes more pronounced over time. The corresponding 1D difference curves [$\Delta f(r; t)$] shown in Figure 1b exhibit peaks with both negative and positive amplitudes: *the negative peaks (shaded blue) represent the depletion of covalent (1.4 Å) and second-nearest neighbor (2.4 Å) distances, whereas positive peaks (shaded red) denote the formation of new internuclear pairs (e.g., those at 1.3 and 1.5 Å and at distances greater than 3.5 Å).*

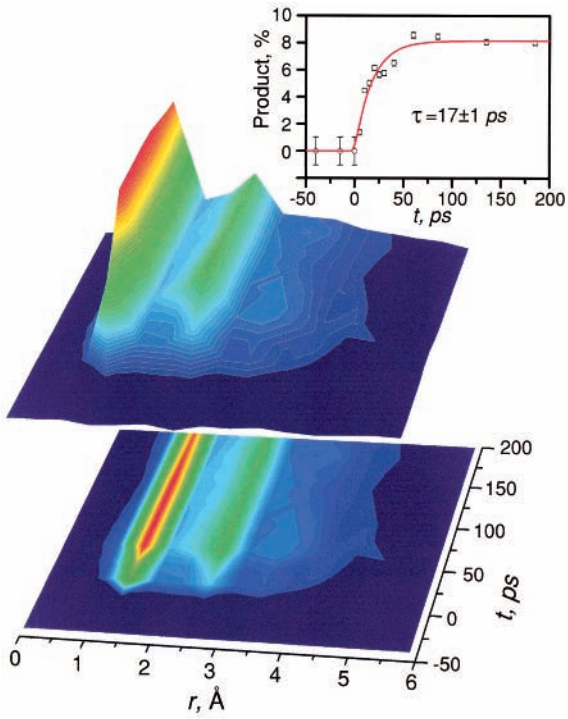

Figure 2. Time-resolved evolution of product-isolated diffraction signals. The product-isolated curves show the formation of product structures following excitation with a femtosecond laser. The inset shows the temporal dependence of the product fraction, which fits a single-component rise (i.e., the formation of the ring-opened structure) and yields a time constant of 17 ± 1 ps. The 2D plot indicates the range of internuclear distances (0−6 Å) and their change as a function of time.

Figure 2 shows the corresponding structural evolution of the "product-isolated" $f(r)$ curves resulting from the product structures alone. The product-isolated curves were obtained by adding the parent diffraction signal (scaled by the fraction of parent molecules depleted at each time point) to the diffraction-difference curves, thereby canceling out the parent contribution. Except for their relative intensities, the shapes of the product-isolated curves were nearly indistinguishable over time. A least-squares fit of the time-dependent product fractions gave the time constant of 17 ± 1 ps, which was essentially independent of the details of the structural model for the products used to fit the experimental data. These results, in conjunction with the difference curves in Figure 1b, clearly indicate the change of the molecular structure over time, primarily manifested as the formation of new C−N and C−C distances.

To consider the various reaction channels, the UED data were fit to a series of structural models. Scheme 1 depicts some structures proposed in the literature for the photochemistry of such aromatic molecules: in the gas phase (Dewar- and Hückel-type isomers[18] and C_4H_4 + HCN fragmentation[18,20]); liquid phase (Dewar isomer,[21] azaprefulvene isomer[22]); matrixes (Dewar isomer[23−25,22] and C_4H_4+HCN fragmentation[23,25]); and quantum chemical calculations.[18] Figure 3 shows the comparison between the experimental product-isolated $f(r)$ curves averaged over four time slices (from +60 to +185 ps) and the corresponding theoretical curves for various trial structures (adjusted for excess internal energy). The poor agreement between theory and experiment for the vibrationally hot Kekulé, Dewar, Hückel, azaprefulvene, and C_4H_4 + HCN fragmentation channels precludes these structures from being involved in the dominant reaction channel on our time scale (Figure 3). When a mixture

SCHEME 1: Relevant Molecular Structures for Five of the Possible Pyridine Reaction Channels Considered in This Work

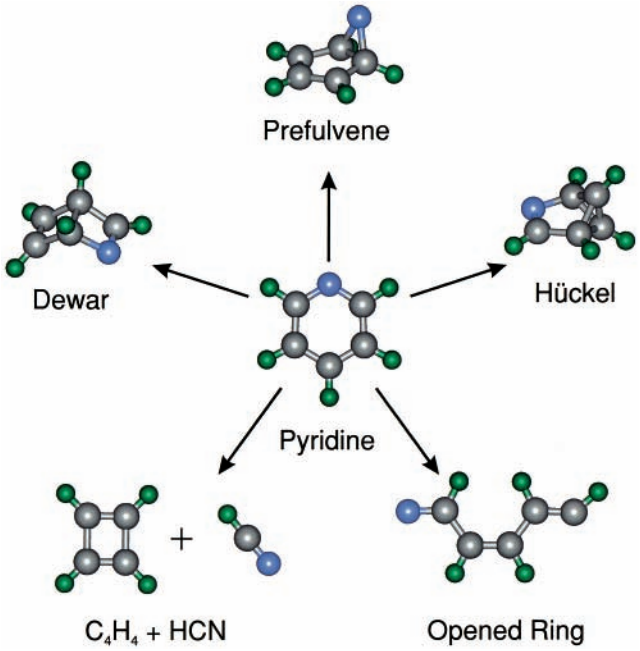

of Dewar, Hückel, and vibrationally "cold" (403 K) ring-opened structures was fit to the experimental $f(r)$ curve, this multicomponent fit indicated that ring opening was the major channel, with the isomerization to the Dewar structure being the minor one; the contribution of the Hückel isomer is vanishingly small.

A superior fit was obtained using just the ring-opened structure albeit with increased internal energy, manifested by mean amplitudes of vibration ~70−100% higher than those of the cold structure at 403 K. These higher vibrational amplitudes, reflected as peak broadening in the experimental $f(r)$ curves, could easily result from a nonthermal (non-Boltzmann) population in the molecule's vibrational degrees of freedom, as has been shown recently by our UED investigations of pericyclic reactions.[14] In the presence of such hot ring-opened structures, the relative fractions of the Dewar and Hückel structures become negligible in a multicomponent fit. These results establish that the primary product is a hot ring-opened structure.

Figure 4 shows the ring-opened structure following least-squares refinement of vibrational amplitudes[26] and internuclear distances[27] along with the corresponding modified molecular scattering [$sM(s)$] and $f(r)$ curves. The features of this refined structure are consistent with the diffraction-difference curves of Figure 1; for instance, the C1−N distance of ~5.23 Å and C1−C5 distance of ~4.33 Å correspond to the emergence of long internuclear separations and, hence, the loss of covalent and next-nearest neighbor distances. As shown in Figure 4, the best-fit covalent bond distances and all but one of the angles agree well with quantum chemical calculations performed in this laboratory (shown in parentheses). The primary exception is one of the skeletal torsional angles which, with a best-fit value of ~123° (instead of 180°), distorts the planarity of the predicted ring-opened structure and places the N atom ~60° above the plane defined by the carbon skeleton. Because UED measures the structure representing all molecules, this result must reflect the multiple torsional conformations, in concordance with a highly flexible structure.[14] The excellent agreement between theory and experiment in Figure 4 and the rejection of other structural possibilities in Figure 3 underscore the sensitivity of

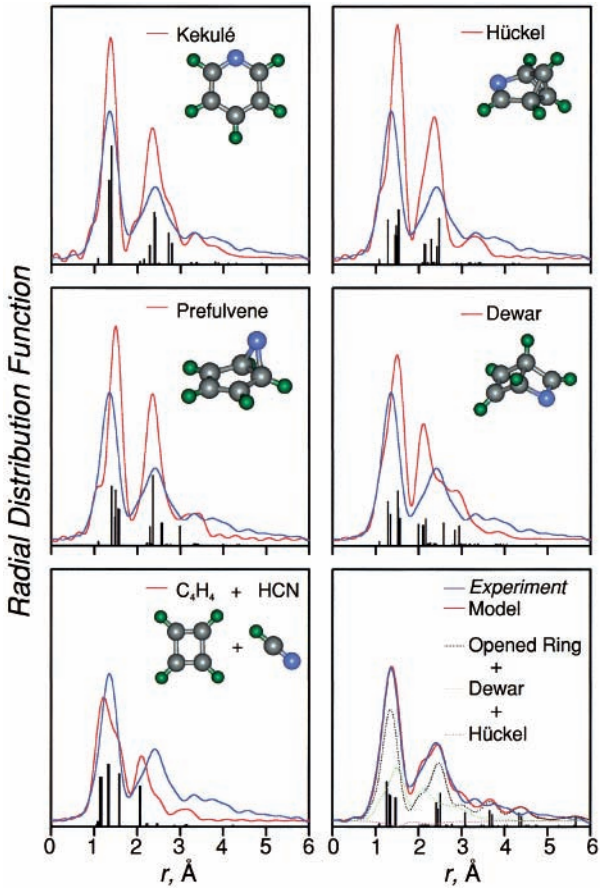

Figure 3. Structure determination of reaction product. Comparisons of the experimental product-isolated radial distribution $f(r)$ curve (blue) to normalized theoretical $f(r)$ curves (red), predicted for the product structures resulting from various possible reaction channels. Discrepancies between theory and experiment are evident for all channels but one: that of the ring-opened structure with minor contributions from the valence isomers; see text.

UED to discriminate among a multitude of structures involved in the dominant channels of the change.

Our UED observations for pyridine are directly relevant to the so-called "channel three" nonradiative process observed in many aromatic molecules. It is interesting to compare the observed UED structural dynamics with the many spectroscopic experimental results and calculations for this prototype molecule. The 0−0 bands for $S_0 \rightarrow S_1(n, \pi^*)$ and $S_0 \rightarrow S_2(\pi, \pi^*)$ absorptions in pyridine vapor occur at 34 769 cm^{-1} and 38 350 cm^{-1}, respectively;[32] accordingly, our pump photon at ~267 nm excites the molecules into the higher vibrational levels of $S_1(n, \pi^*)$ with an excess energy of ~2700 cm^{-1}, well above the ~1600 cm^{-1} threshold for channel three behavior in pyridine. Significant contribution from multiphoton processes was not evident because no fragmentation channels were observed (as would be expected based on previous reports in the literature[18,20]) and because the laser power was not very high (~5×10^{11} W/cm^2), given that a resonant transition of pyridine was excited. Historically, various explanations have been invoked to account for the channel three behavior, and our UED data does not support such scenarios as (i) direct $S_1 \rightarrow S_0$ internal conversion, which would land the molecule on the electronic ground state with a concomitant increase in internal energy, making it vibrationally hot. However, as seen in Figure 3, we do not observe the hot parent structure despite the proven sensitivity of our UED apparatus to hot molecules[14] and (ii) valence isomerization-mediated internal conversion (e.g.,

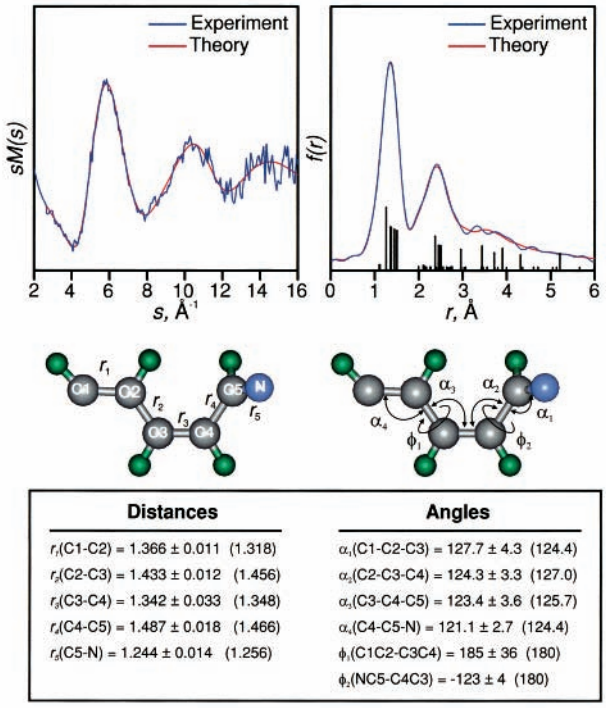

Figure 4. Refined structure determination from diffraction images. Shown on top are the experimental diffraction (time-averaged) curves of products alone (blue) compared to theoretical curves corresponding to the ring-opened structure with mean *l* values ~70−100% larger than those obtained at 403 K (red). The modified molecular scattering *sM*(*s*) curves are shown on the left, and the corresponding radial distribution *f*(*r*) curves are shown on the right. At the bottom are shown refined structural parameters for the ring-opened product compared to the corresponding values predicted by quantum chemical calculations (shown in parentheses). Distances are in ångströms, and angles are in degrees.

via the Dewar, Hückel, or azaprefulvene structures), which can also be ruled out based on the poor fits to these valence isomers (Figure 3).

The observed ring-opened structure is dominant in the "direct" transition from the excited pyridine molecule to the diradical. In principle, there are three possible pathways which involve the conversion of the S_1 population to the hot ground state (or another isomer or triplet state) and then proceed to open the ring; the alternative is to open the ring directly. The molecular structures of pyridine in its hot ground state, its Dewar isomer, and its triplet state are each markedly different from that of the cold (403 K) parent Kekulé structure. Hence, if any of these structures were intermediates in the formation of the ring-opened structure, then our UED data would have revealed the depletion of the population of these structures as the ring-opened structure is formed in 17 ps. The diradical structure thus born directly in its singlet state may then change its spin to the triplet because our quantum chemical calculations predict that these states are nearly degenerate and that their structures are virtually identical.

Femtosecond, time-resolved mass-spectrometric experiments[18] on gas-phase pyridine have revealed a fast decay component of 400 fs, which describes the initial motion on the potential surface of pyridine, and slower components of 3.5 and 15 ps, which were assigned to the formation of Dewar and Hückel isomers, respectively. We note that these experiments were performed just below *both* the apparent channel three threshold and the apparent energy required for ring opening. Thus, our UED results indicate that the observed ring-opening process is dominant in the channel three dynamics of vibrationally hot pyridine. Experiments at different energies will be part of our future research effort.

In conclusion, we have shown the ability of UED to study the fundamental structural dynamics underlying radiationless transitions in complex molecules. Previous reports of UED have elucidated the new limits of temporal and spatial resolution achieved and the isolation of intermediate structures in reactions of known products. Here, for the first time, UED has uncovered a previously unknown structure in the radiationless transition of the prototypical pyridine molecule: this observed ring-opened structure casts new light on the decades-old puzzle of channel three behavior occurring in many aromatic molecules. The advances reported here promise myriad extensions in the studies of transient structures in nonradiative, ultrafast processes.

Acknowledgment. We gratefully acknowledge Hyotcherl Ihee for helpful discussions. We thank E. W.-G. Diau, T. I. Sølling, and C. Kötting for help with the quantum chemical calculations. This work was supported by the National Science Foundation and the Air Force Office of Scientific Research.

References and Notes

(1) Lim, E. C. *Adv. Photochem.* **1997**, *23*, 165.
(2) Avouris, P.; Gelbart, W. M.; El-Sayed, M. A. *Chem. Rev.* **1977**, *77*, 793.
(3) Turro, N. *Modern Molecular Photochemistry*; University Science: Sausalito, CA, 1991.
(4) Villa, E.; Amirav, A.; Lim, E. C. *J. Phys. Chem.* **1988**, *92*, 5393.
(5) Sobolewski, A. L.; Woywood, C.; Domcke, W. *J. Chem. Phys.* **1993**, *98*, 5627.
(6) Palmer, I. J.; Ragazos, I. N.; Bernardi, F.; Olivucci, M.; Robb, M. A. *J. Am. Chem. Soc.* **1993**, *115*, 673.
(7) Yamazaki, I.; Sushida, K.; Baba, H. *J. Chem. Phys.* **1979**, *71*, 381.
(8) Yamazaki, I.; Murao, T.; Yamanaka, T.; Yoshihara, K. *Faraday Discuss. Chem. Soc.* **1983**, *75*, 395.
(9) Otis, C. E.; Knee, J. L.; Johnson, P. M. *J. Phys. Chem.* **1983**, *87*, 2232.
(10) Schubert, U.; Riedle, E.; Neusser, H. J.; Schlag, E. W. *J. Chem. Phys.* **1986**, *84*, 6182.
(11) Parmenter, C. S.; Schuyler, M. W. *Chem. Phys. Lett.* **1970**, *6*, 339.
(12) Williamson, J. C.; Zewail, A. H. *Proc. Natl. Acad. Sci. U.S.A.* **1991**, *88*, 5021.
(13) Ihee, H.; Lobastov, V. A.; Gomez, U.; Goodson, B. M.; Srinivasan, R.; Ruan, C.-Y.; Zewail, A. H. *Science* **2001**, *291*, 458.
(14) Ruan, C.-Y.; Lobastov, V. A.; Srinivasan, R.; Goodson, B. M.; Ihee, H.; Zewail, A. H. *Proc. Natl. Acad. Sci. U.S.A.* **2001**, *98*, 7117.
(15) Dantus, M.; Kim, S. B.; Williamson, J. C.; Zewail, A. H. *J. Phys. Chem.* **1994**, *98*, 2782.
(16) Lobastov, V. A.; Ewbank, J. D.; Schäfer, L.; Ischenko, A. A. *Rev. Sci. Instrum.* **1998**, *69*, 2633.
(17) Pyckhout, W.; Horemans, N.; Vanalsenoy, C.; Geise, H. J.; Rankin, D. W. H. *J. Mol. Struct.* **1987**, *156*, 315.
(18) Zhong, D.; Diau, E. W.-G.; Bernhardt, T. M.; Feyter, S. D.; Roberts, J. D.; Zewail, A. H. *Chem. Phys. Lett.* **1998**, *298*, 129.
(19) Ihee, H.; Cao, J.; Zewail, A. H. *Chem. Phys. Lett.* **1997**, *281*, 10.
(20) Prather, K. A.; Lee, Y. T. *Isr. J. Chem.* **1994**, *34*, 43.
(21) Wilzbach, K. E.; Rausch, D. J. *J. Am. Chem. Soc.* **1970**, *92*, 2178.
(22) Chachisvilis, M.; Zewail, A. H. *J. Phys. Chem. A* **1999**, *103*, 7408.
(23) Chapman, O. L.; McInstosh, C. L.; Pacansky, J. *J. Am. Chem. Soc.* **1973**, *95*, 614.
(24) Johnstone, D. E.; Sodeau, J. R. *J. Phys. Chem.* **1991**, *95*, 165.
(25) Kudoh, S.; Takayanagi, M.; Nakata, M. *J. Photochem. Photobio. A: Chem.* **1999**, *123*, 25.
(26) Mean amplitudes of vibration were estimated using empirical equations given in refs 28 and 29; vibrationally excited product structures were modeled by parametrically increasing these *l* values to account for higher internal energies[14,30] predicted by quantum chemical calculations. Predictions for energies and molecular structures of the relevant species (those calculated previously[18] and in this work) were obtained using a commercial computational chemistry package;[31] details of the quantum chemical calculations will be provided in a separate publication. Vibrational frequencies and geometries were calculated using density functional theory

(DFT) methods (at the B3LYP/6-311G** level), and energies were calculated using a variety of DFT and ab initio methods.

(27) Extrapolated l values were also used to relate r_e (the geometrically consistent, equilibrium internuclear distance at the potential minimum) to r_a (the internuclear distance measured by electron diffraction), using the equation $r_a \approx r_e + (3/2)al^2 + dr - l^2/r$, where a is the anharmonicity constant for the bond and dr is the small correction due to centrifugal distortion.[30] To obtain refined molecular structures from experimental UED data, geometrically consistent molecular structures were built using internal coordinates of a given molecule, defining the configuration space. A Monte Carlo sampling procedure was then applied to locate χ^2 minima within the configuration space, followed by least-squares refinement of the molecular structure.[14] In the final refinement of the RO structure, the overall connectivity of the theoretical RO structure was assumed.

(28) Mastryukov, V. S.; Cyvin, S. J. *J. Mol. Struct.* **1975**, *29*, 15.

(29) Mastryukov, V. S.; Osina, E. L.; Vilkov, L. V.; Cyvin, S. *J. Struct. Chem.* **1976**, *17*, 64.

(30) Hargittai, I.; Hargittai, M. *Stereochemical Applications of Gas-Phase Electron Diffraction*; VCH: New York, 1988.

(31) Frisch, M. J.; Trucks, G. W.; Schlegel, H. B.; Scuseria, G. E.; Robb, M. A.; Cheeseman, J. R.; Zakrzewski, V. G.; Montgomery, J. A., Jr.; Stratmann, R. E.; Burant, J. C.; Dapprich, S.; Millam, J. M.; Daniels, A. D.; Kudin, K. N.; Strain, M. C.; Farkas, O.; Tomasi, J.; Barone, V.; Cossi, M.; Cammi, R.; Mennucci, B.; Pomelli, C.; Adamo, C.; Clifford, S.; Ochterski, J.; Petersson, G. A.; Ayala, P. Y.; Cui, Q.; Morokuma, K.; Malick, D. K.; Rabuck, A. D.; Raghavachari, K.; Foresman, J. B.; Cioslowski, J.; Ortiz, J. V.; Stefanov, B. B.; Liu, G.; Liashenko, A.; Piskorz, P.; Komaromi, I.; Gomperts, R.; Martin, R. L.; Fox, D. J.; Keith, T.; Al-Laham, M. A.; Peng, C. Y.; Nanayakkara, A.; Gonzalez, C.; Challacombe, M.; Gill, P. M. W.; Johnson, B. G.; Chen, W.; Wong, M. W.; Andres, J. L.; Head-Gordon, M.; Replogle, E. S.; Pople, J. A. *Gaussian 98*, revision A.9; Gaussian, Inc.: Pittsburgh, PA, 1998.

(32) Innes, K. K.; Ross, I. G.; Moomaw, W. R. *J. Mol. Spectrosc.* **1988**, *132*, 492.